Phonon dispersion in GaAs

1990 J. Phys.: Condens. Matter 2 1457

(http://iopscience.iop.org/0953-8984/2/6/006)

J. Phys.: Condens. Matter 2 (1990) 1457–1474. Printed in the UK

Phonon dispersion in GaAs

D Strauch† and B Dorner‡

† Theoretische Physik, Universität Regensburg, D-8400 Regensburg, Federal Republic of Germany

‡ Institut Laue-Langevin, F-38042 Grenoble Cedex, France

Received 12 May 1989, in final form 25 August 1989

Abstract. We have determined the phonon dispersion curves in GaAs at 12 K for wavevectors along the six directions

$$\Gamma\text{–}(\Delta)\text{–X–}(\Sigma)\text{–}\Gamma\text{–}(\Lambda)\text{–L–X–}(Z)\text{–W–}(Q)\text{–L}$$

by high-precision inelastic neutron scattering. Various existing lattice-dynamical models are used to reproduce the experimental data. The relative merits and drawbacks of these models are discussed.

1. Introduction

Phonon dispersion curves of gallium arsenide at room temperature (with a few results at 95 K) were determined by Dolling and Waugh (1965, Waugh and Dolling 1963) some twenty years ago. Quantum-mechanical calculations (see, e.g., Kunc and Hagège 1985 and Falter *et al* 1985) are now sufficiently far advanced that quantitative results can be obtained. On the other hand, these methods require extensive use of computer time, and some of them are limited to high-symmetry phonons. Thus, realistic lattice-dynamical models still seem to be indispensable, and only precise experimental information is able to discriminate between competing models and to serve as a basis for the design of new ones.

The present study was ultimately motivated by the partial disagreement between the phonon dispersion curves determined by inelastic neutron scattering (Dolling and Waugh 1965) and those deduced from Raman scattering experiments on GaAs/AlAs superlattices (Sood *et al* 1985, 1986, Molinari *et al* 1986, Jusserand and Paquet 1986, Ishibashi *et al* 1986, Fasol *et al* 1988), which are usually conducted at low temperatures (see also the recent review by Jusserand and Cardona 1989).

This, together with the improvement of instrumentation and of crystal preparation makes a repeat investigation appear sensible, particularly at low temperatures. It is hoped that an extension and an improvement of the experimental data may lead to the construction of a physical model for the lattice dynamics of III–V compounds, which will also be a useful guideline for the development of the quantum-mechanical theory.

The experimental details are described in § 2, and the results of these experiments are given in § 3. In § 4 we compare the experimental results with those of various model calculations; in the first part, § 4.1, the experimental phonon dispersion curves are compared to those resulting from a least-squares fit of the parameters of various models,

0953-8984/90/061457 + 18 $03.50

and further lattice-dynamical properties are compared among the models and with experiment in the subsections following 4.1. Section 5 summarises our results.

2. Experiment

We have carried out inelastic neutron-scattering experiments using the three-axis spectrometer IN8 at the high-flux reactor of the ILL. Cu(220) was used as a monochromator for higher (>2 THz) and Cu(111) for the lower energy transfer; the analyser was pyrolytic graphite; collimator divergences were 40′, 40′, 60′, 60′. The final wavevector was kept constant at $k_f = 2.662$ Å^{-1}, where higher-order radiation (if any) was reduced by a graphite filter in front of the analyser. Constant-$\boldsymbol{Q}$ scans were recorded for wavevectors lying in the (001) and ($\bar{2}11$) planes in six different directions which are depicted in figure 1.

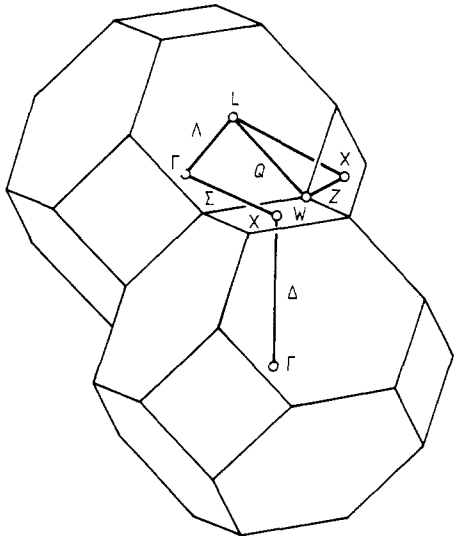

Figure 1. Two different Brillouin zones with the wavevector directions investigated in the present study.

The crystal, 4.5 cm high and 5 cm in diameter, was kindly supplied by Dr Stath of Siemens AG. The crystal was kept in a Displex cryostat at 12 K. A lattice constant of $a = 5.637$ Å gave the optimal alignment of the sample and the instrument.

3. Results

The experimental scattering spectra were analyzed by a Gaussian (plus constant background) least-squares fit. The fitted peak centres were taken as the phonon frequencies. These are listed in tables 1 to 6. The systematic error is estimated to be 0.02 THz, even though the uncertainty of the relative frequency values for adjacent wavevectors is probably lower by half an order of magnitude. Where the experimental error turned out to be larger than 0.02 THz, the estimated value is given in the tables.

Table 1. Phonon frequencies at $T = 12$ K for wavevectors along $[00\zeta]$ (Γ–(Δ)–X). The error in the last digit is 2 unless otherwise set in brackets. The symbols * and + mark those wavevectors which are used in the fitting for the models with suffix 5 and 3 respectively.

ζ	TA	LA	TO	LO
0.0 *+	—	—	8.13	8.79
0.1 +	0.64	0.91	8.11	8.78(3)
0.15	—	1.38	—	—
0.2 *+	1.17	1.79	8.04	8.80
0.3 +	1.60	2.55	7.94	8.68
0.4 *+	1.93	3.32	7.85	8.59
0.5 +	2.17	4.04	7.77	8.46
0.6 *+	2.32	4.72	7.71	8.28
0.7 +	2.40	5.35	7.64	8.05
0.75	2.42	5.65	—	—
0.8 *+	2.43	5.93	7.73	7.75
0.85	2.44	6.18	—	7.59
0.9 +	2.44	6.43	7.73	7.38
0.925	—	6.53	—	—
0.95	2.45	6.62	—	7.25
0.975	—	6.70	—	—
1.0 *+	2.45	6.75	7.69	7.20

Table 2. Same as table 1 but for wavevectors along $[\xi\xi 0]$ (Γ–(Σ)–X).

ξ	TA	I	II	TO	III	IV
0.0	—	—	—	8.13	8.13	8.79
0.025	—	—	—	—	—	8.81
0.05	—	—	—	—	8.14	8.75
0.1 +	0.66	—	1.40	8.05	8.13	8.73
0.15	—	1.16	1.97	—	8.09	8.68
0.2 *+	1.20	1.54	2.56	8.00	8.03	8.58
0.25	—	1.88	3.04	—	7.95	8.48
0.3 +	1.65	2.22	3.49	7.93	7.88	8.37
0.35	—	2.45	—	—	7.72	8.27
0.4 *+	2.01	2.71	4.27	7.84	7.58	8.22
0.45	—	2.92	—	—	7.41	8.21
0.5 +	2.25	3.11	4.92	7.77	7.25	8.24
0.55	—	3.27	5.19	—	—	8.21
0.6 *+	2.40	3.39	5.46	7.71	6.91	8.19
0.65	—	3.45	5.71	—	—	8.17
0.7 +	2.46	3.44	5.92	7.70	6.64	8.15
0.75	2.43	3.35	6.11	—	6.63	8.08
0.8 *+	2.44	3.17	6.25	7.69	6.77	8.01
0.85	—	2.92	6.37		6.93	7.92
0.9 +	2.43	2.68	6.54	7.69	7.16	7.82
0.95	—	—	—	—	7.24	7.72
1.0	2.45	2.45	6.75	7.69	7.20	7.69

Table 3. As table 1, but for wavevectors along [ξξξ] (Γ–(Λ)–L).

ξ	TA	LA	TO	LO
0.0	—	—	8.13	8.79
0.025	—	—	—	8.79
0.05	0.44	0.87	—	8.78
0.075	—	—	—	8.76
0.1 *+	0.83	1.72	8.10	8.73
0.15	1.15	2.48	—	8.64
0.2 *+	1.40	3.23	7.92	8.51
0.25	1.60	3.93	—	8.32
0.3 *+	1.73	4.56	7.93	8.16
0.35	1.82	5.14	—	7.82
0.4 *+	1.87	5.64	7.89	7.57
0.45	1.90	6.04	—	7.34
0.475	—	6.17	—	7.28
0.5 *+	1.90	6.20	7.90	7.25

Table 4. As table 1, but for wavevectors along $[\frac{1}{2}+\xi, \frac{1}{2}+\xi, \frac{1}{2}-\xi]$ (L–X).

ξ	I(TA)	II	III	IV	V(TO)	VI
0.0	1.90	1.90	6.20	7.25	7.90	7.90
0.05	1.91(3)	2.08(3)	—	7.27	—	—
0.1 *	2.02(4)	2.29(3)	5.84(2)	7.20	7.80	8.03(3)
0.15	2.15(5)	2.70	5.59(3)	7.11	7.74	8.09
0.2*	2.26(4)	3.00	5.37	7.09	7.76	8.10
0.25	2.34	3.14	5.46(5)	—	7.71	8.07
0.3 *	2.39	3.09	5.57	7.10	7.71	8.04
0.35	2.39	2.80(5)	5.90	—	7.69	7.97
0.4 *	2.35	2.54(5)	6.28	—	7.69	7.85(4)
0.45	—	—	6.60	7.16	7.68	—
0.5	2.45	2.45	6.75	7.20	7.69	7.69

Table 5. As table 1, but for wavevectors along $[1, 1-\xi, 0]$ (X–(Z)–W).

ξ	I	II	III	IV	V	VI
0.0	2.45	2.45	6.75	7.20	7.69	7.69
0.025	—	—	6.73	7.18	—	—
0.05	—	—	6.70	7.15	—	—
0.075	—	—	6.67	7.12	—	—
0.1	2.43	2.55	6.63	7.07	—	—
0.15	2.47	2.66	6.55	6.97	—	—
0.2	2.57	2.83	6.45	6.84	7.64(5)	7.92(5)
0.25	—	—	6.35	6.71	—	—
0.3	2.77	3.12	6.25	6.56	7.69(3)	7.80(4)
0.35	2.86	3.24	6.15	6.44	—	—
0.4	2.97	3.36	6.05	6.33	7.68	8.06(3)
0.425	—	—	6.00	6.27	—	—
0.45	3.02	3.40	5.95	6.23	—	—
0.475	—	—	5.91	6.21	—	—
0.5	3.02	3.41	5.92	6.25	7.68	8.06(3)

Table 6. As table 1, but for wavevectors along $[1-\xi, \frac{1}{2}, \xi]$ (W–(Q)–L).

ξ	I	II	III	IV	V	VI
0.0 *	3.02	3.41	5.92	6.25	7.68	8.06
0.05	2.99	3.42	5.99	6.37	7.76	8.02
0.1 *	2.88	3.41	5.85	6.51	7.73	8.07
0.15	2.77	3.41	5.72	6.67	7.75	8.08
0.2 *	2.60	3.31	5.64	6.79	7.81	8.13
0.25	2.46	3.16	5.61	6.95(3)	7.90(4)	8.12
0.3 *	2.29	2.90	5.65	7.00(3)	7.87(4)	8.09
0.35	2.13	2.61	5.79	7.16	—	—
0.4 *	2.01	2.27	5.97	7.20	7.92(3)	8.14(4)
0.45	1.91(5)	2.00	6.16	7.29	7.83	8.02(5)
0.5	1.90	1.90	6.20	7.25	7.90	7.90

Working with fixed final wavevector $\boldsymbol{k}_f$ has the advantage (Dorner 1972) that the experimental scattering intensities (the area under the fitted Gaussian curves) are directly comparable to the scattering function

$$S(\boldsymbol{Q}, \omega) = \frac{\hbar}{2}\frac{1+n_\omega}{\omega}\sum_{gqj}\delta(\boldsymbol{q}+\boldsymbol{g}-\boldsymbol{Q})\delta[\omega(qj)-\omega] \times \left|\sum_\kappa \boldsymbol{Q}\cdot\boldsymbol{e}(\kappa|qj)\exp[-i\boldsymbol{Q}\cdot\boldsymbol{R}(\kappa)]\exp(-W_\kappa)b_\kappa/\sqrt{M_\kappa}\right|^2. \quad (1)$$

Here, $\omega = \omega_i - \omega_f$ and $\boldsymbol{Q} = \boldsymbol{k}_i - \boldsymbol{k}_f$ are respectively the energy and momentum transfer; b_κ and M_κ are respectively the scattering length and mass of the atom of type κ; n_ω is the Bose factor; the eigenvector $\boldsymbol{e}(\kappa|qj)$ is related to the atomic displacement $\boldsymbol{u}(l\kappa)$ by

$$\boldsymbol{u}(l\kappa) = \sum_{qj}\sqrt{\frac{\hbar}{2NM_\kappa\omega(qj)}}\,\boldsymbol{e}(\kappa|qj)\exp[i\boldsymbol{Q}\cdot\boldsymbol{R}(l)].$$

The exponent in the Debye-Waller factor $\exp(-W_\kappa)$ can be written as

$$W_\kappa = \frac{1}{6}\hat{Q}^2\langle u^2(l\kappa)\rangle = \frac{1}{6}Q^2\frac{1}{N}\sum_{qj}\frac{\hbar}{2\omega(qj)M_\kappa}|\boldsymbol{e}(\kappa|qj)|^2(1+2n_{\omega(qj)}) \quad (2)$$

which is independent of the lattice cell l. The scattering intensity contains information about the phonon eigenvectors $\boldsymbol{e}(\kappa|qj)$ and can be used for the symmetry assignment of the phonons.

In addition to the data for wavevectors $\boldsymbol{q}$ along the main symmetry directions we have also taken data along three other directions, since for these wavevectors major discrepancies between different model calculations had become apparent.

The symmetry assignment for the main symmetry directions is known (Dolling and Waugh 1965) and has been confirmed from scattering intensities. For $\boldsymbol{q}$ along the L–X direction the assignment has been inferred from the unanimous results of model calculations, see also the next section. For $\boldsymbol{q}$ along the W–L direction there is only one irreducible representation. For $\boldsymbol{q}$ along the X–W direction there are two irreducible representations, with three modes in each. In principle, the symmetry could be assigned to these modes by an analysis of their scattering intensities in different Brillouin zones,

but limitations of instrument time did not allow this. However, some remarks can be found in § 4.5.

For wavevectors along $[0, 0, \zeta]$, $[\xi, \xi, \xi]$, and $[\xi, \xi, 0]$, our frequencies (at12 K) are in general agreement with the 95 K data of Dolling and Waugh (1965) and somewhat higher than their room temperature data. However, the error is now appreciably reduced, in particular for the optical modes where the data are now more precise by about an order of magnitude.

4. Comparison with model results

4.1. Phonon dispersion curves and model parameters

The experimental dispersion curves have been analysed with the help of phenomenological lattice-dynamical models. These models are described in terms of charges and force constants, from which the elements of the dynamical matrix can be derived. We have investigated a total of eight lattice-dynamical models. These are the four shell models of Dolling and Waugh (1965), a deformable-dipole model (DDM) (Kunc *et al* 1975b), a rigid-ion model (RIM) (Kunc *et al* 1975a), the overlap valence shell model (OSM) (Kunc and Bilz 1976a, b), and the bond-charge model (BCM) (Weber 1974, 1977, Rustagi and Weber 1976). These (and other) models are reviewed by Sinha (1973). Computer programs for these models (except for the BCM) are described by Kunc and Nielsen (1979a, b).

The experimental data have been used to readjust the parameters of these models by minimising the quantity

$$\chi^2 = \frac{1}{N_d - N_p} \sum_{q,j} \left(\frac{\nu_{th}(q,j) - \nu_{exp}(q,j)}{\sigma_{exp}(q,j)} \right)^2. \tag{3}$$

Table 7. Deformation-dipole and rigid-ion model parameters.

Parameter	D[a]	D5	D3	R[a]	R5	R3
$-\alpha = A$	−8.652	−8.264 ± 0.014	−8.094 ± 0.027	−7.956	−8.060 ± 0.011	−8.049 ± 0.008
$-\beta = B$	−5.969	−8.074 ± 0.197	−2.994 ± 0.086	−3.252	−3.161 ± 0.033	−3.637 ± 0.037
$-\mu_1 = C_1$	−0.610	−0.282 ± 0.035	−0.647 ± 0.018	−0.346	−0.422 ± 0.010	−0.398 ± 0.009
$-\nu_1 = D_1$	0.516	−0.058 ± 0.031	0.042 ± 0.030	0.485	0.755 ± 0.025	0.523 ± 0.029
$-\delta_1 = E_1$	1.110	2.256 ± 0.081	1.527 ± 0.026	1.782	1.898 ± 0.013	1.942 ± 0.018
$-\lambda_1 = F_1$	−2.164	−0.646 ± 0.085	−1.777 ± 0.028	−2.291	−1.903 ± 0.018	−1.893 ± 0.017
$-\mu_2 = C_2$	−0.491	−0.183 ± 0.010	−0.628 ± 0.010	−0.901	−0.719 ± 0.009	−0.908 ± 0.049
$-\nu_2 = D_2$	−1.669	−0.419 ± 0.044	−0.172 ± 0.030	−2.410	−2.110 ± 0.018	−1.933 ± 0.023
$-\delta_2 = E_2$	0.104	1.797 ± 0.029	0.991 ± 0.030	1.630	1.632 ± 0.010	1.479 ± 0.021
$-\lambda_2 = F_2$	2.267	4.126 ± 0.047	3.413 ± 0.029	3.924	3.614 ± 0.013	3.818 ± 0.014
Z_1	−0.094	2.009 ± 0.050	0.111 ± 0.029	0.658	0.625 ± 0.006	0.626 ± 0.089
γ_1	0.395	−0.421 ± 0.011	0.531 ± 0.018	—	—	—
γ_2	0.055	−0.602 ± 0.037	−0.133 ± 0.020	—	—	—
α_1	0.003	−0.006 ± 0.001	−0.056 ± 0.007	—	—	—
α_2	0.180	0.064 ± 0.002	0.054 ± 0.003	—	—	—
χ^2		26.5	17.3		47.8	19.4

[a] Kunc *et al* (1975b) give values in cgs units, see text.

Table 8. Shell model B parameters.

Parameter	B(i)[a]	B5(i)	B3(i)	B(ii)[a]	B5(ii)	B3(ii)
α_R	20.41	13.68 ± 0.18	12.70 ± 0.15	20.52	15.67 ± 0.31	14.59 ± 0.17
Z_1	0.049	−0.242 ± 0.015	−0.112 ± 0.016	0.040	0.130 ± 0.013	0.074 ± 0.010
π_1	0.018	0.038 ± 0.001	0.034 ± 0.001	0.032	0.047 ± 0.002	0.065 ± 0.002
π_2	0.025	0.025 ± 0.001	0.037 ± 0.002	0.015	0.016 ± 0.001	0.018 ± 0.001
d_1	0.812	0.706 ± 0.014	0.562 ± 0.013	1.183	1.061 ± 0.021	1.111 ± 0.015
d_2	1.043	0.678 ± 0.012	0.732 ± 0.019	0.743	0.590 ± 0.011	0.552 ± 0.007
α_S/α_R	1.565	2.378 ± 0.055	2.704 ± 0.077	1.531	1.876 ± 0.045	1.893 ± 0.030
$\gamma_R = \gamma_T = \gamma_S$	0.461	0.551 ± 0.005	0.574 ± 0.005	0.432	0.547 ± 0.006	0.549 ± 0.005
μ	−0.909	0.128 ± 0.019	0.237 ± 0.016	−0.922	−0.054 ± 0.037	−0.001 ± 0.019
λ	−1.457	−0.902 ± 0.040	−0.907 ± 0.038	−1.599	−1.370 ± 0.058	−1.250 ± 0.035
ν	−0.233	0.399 ± 0.012	0.384 ± 0.012	−0.165	0.205 ± 0.023	0.205 ± 0.015
δ	1.000	−0.468 ± 0.018	0.234 ± 0.017	0.750	0.350 ± 0.017	0.177 ± 0.018
χ^2		23.5	20.5		28.8	25.7

[a] Dolling and Waugh (1965).

N_d is the number of experimental data points; N_p the number of adjusted model parameters; $\nu_{th}(\boldsymbol{q}, j)$ and $\nu_{exp}(\boldsymbol{q}, j)$ are the model and experimental frequencies, respectively, for wavevector $\boldsymbol{q}$ and branch index j, and σ_{exp} is the experimental uncertainty (typically 0.02 THz). (If a quantity other than χ^2 is minimised the parameters will turn out to be somewhat different, of course.)

In two different runs a selected set of wavevectors $\boldsymbol{q}$ along either three or five directions has been included in the sum in equation (3) amounting to a total of $N_d = 115$ and $N_d = 119$ frequencies, respectively. The corresponding models are denoted in the tables by a suffix 3 and 5, respectively. The wavevectors are selected to approximate an evenly spaced set so that different parts of the Brillouin zone contribute to (3) with

Table 9. Shell model C parameters.

Parameter	C(i)[a]	C5(i)	C3(i)	C(ii)[a]	C5(ii)	C3(ii)
α_R	19.54	9.79 ± 0.15	10.25 ± 0.24	19.67	10.25 ± 0.17	11.12 ± 0.24
Z_1	0.031	−0.384 ± 0.039	−0.418 ± 0.036	0.018	0.752 ± 0.025	0.625 ± 0.021
π_1	0.024	0.085 ± 0.004	0.083 ± 0.005	0.075	0.013 ± 0.002	0.041 ± 0.004
π_2	0.062	0.047 ± 0.008	0.039 ± 0.006	0.014	0.057 ± 0.003	0.051 ± 0.003
d_1	0.882	0.237 ± 0.035	0.332 ± 0.049	1.588	0.269 ± 0.027	0.546 ± 0.028
d_2	1.474	0.460 ± 0.048	0.484 ± 0.057	0.714	0.481 ± 0.027	0.535 ± 0.030
α_S/α_R	1.267	0.973 ± 0.325	1.904 ± 0.250	1.267	3.430 ± 0.260	1.709 ± 0.102
γ_R	0.216	0.507 ± 0.014	0.458 ± 0.015	0.222	0.539 ± 0.017	0.409 ± 0.023
γ_T	0.026	−0.615 ± 0.175	−0.511 ± 0.169	0.043	−0.397 ± 0.089	−0.582 ± 0.082
γ_S	−0.244	−6.830 ± 2.710	−1.960 ± 0.380	−0.133	−0.163 ± 0.112	−1.380 ± 0.170
μ	−0.800	0.428 ± 0.022	0.405 ± 0.032	−0.815	0.399 ± 0.017	0.304 ± 0.029
λ	−1.967	−0.542 ± 0.066	−0.535 ± 0.082	−1.941	−0.136 ± 0.048	−0.242 ± 0.057
ν	0.750	0.997 ± 0.069	1.018 ± 0.074	0.736	1.062 ± 0.050	1.264 ± 0.072
δ	0.750	0.613 ± 0.022	0.522 ± 0.024	0.550	0.736 ± 0.025	0.747 ± 0.031
χ^2		14.7	12.0		16.6	11.4

[a] Dolling and Waugh (1965).

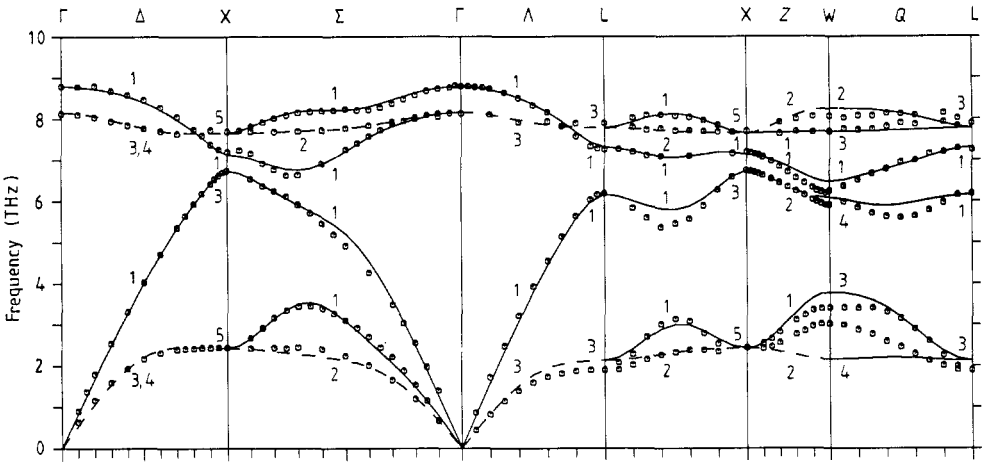

Figure 2. Phonon dispersion curves for GaAs. The experimental data at $T = 12$ K are given by the crosses; the experimental uncertainty is typically 0.02 THz (less than the height of the crosses). The lines give the results of model calculations using the rigid-ion model RIM3. The letters R on top of the figure gives the notation for the symmetry directions or points, and the numbers i refer to the symmetry representations R_i of the corresponding branches or points.

roughly equal weight. Since in the X–W direction the symmetries of the different branches could not be determined (§ 4.5), these data have not been used at all in the minimisation procedure. (The data for this latter direction will turn out to serve as an interesting testing ground for the various models, cf §§ 4.5 and 4.6.) The resulting parameters and their variances are listed in tables 7–11 along with the originally published numbers (see, e.g., chapter 14 of Press *et al* (1986) for the meaning of the variances in the context of non-linear least-squares fitting and non-standard experimental deviations).

Dispersion curves calculated from these models are shown in figures 2–6 together with the experimental data.

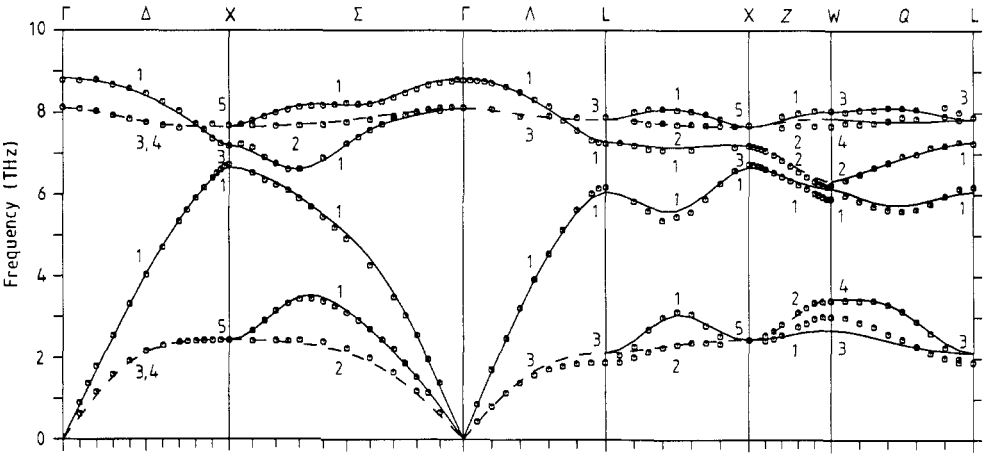

Figure 3. As figure 2, but the model calculations are with the 14-parameter shell model C3(ii).

4.1.1. Rigid-ion model (RIM). In the rigid-ion model, short-range forces to nearest (α, β) and second-nearest neighbours (μ, ν, λ, δ) and Coulomb forces between the (point) ions are included. This notation of the force constants is due to Herman (1959). A model with short-range force constants out to third neighbours is presently investigated by Bross (1989). The model parameters obtained from a fit to our dispersion curves are very close to those of Kunc *et al* (1975b), see table 7. Fitting to five rather than three wavevector directions does not alter the numbers to any significant extent. From the covariance matrix the strongest correlation is between the parameters β and Z_1. The originally published force constants are in cgs units; the conversion factor is $e^2/v = 5117$ dyn cm^{-1} with the lattice constant of $a = 5.65$ Å as used by Kunc *et al* (1975b).

The dispersion along the Δ direction, in particular that of the LA and LO branch near the X point, is, surprisingly enough, well reproduced by the RIM3, see figure 2. However, serious discrepancies occur near the L point and in particular near the W point. Some improvement near the W point is possible (RIM5) at the expense of worse overall agreement.

4.1.2. Shell models (B(i) to C(ii)). The shell model has originally been designed for and applied to the lattice dynamics of ionic crystals (Cochran 1959, Woods *et al* 1960, 1963). In the shell model the ions are assumed to be electrically and mechanically deformable. The respective polarisabilities π_i and d_i ($i = 1, 2$ for Ga and As) are related to electronic-shell charges Y_i and force constants k_i by which a shell is bound to its core. The large number of parameters required for a reasonable description of the dispersion curves in homopolar crystals makes the application of this model to these substances questionable.

The four shell models B(i), B(ii), C(i), and C(ii) of Dolling and Waugh (1965) differ from each other in that the ratio γ of the diagonal to off-diagonal force constant elements (equal to α/β in Herman's (1959) notation) for core–core, core–shell, and shell–shell force constants (with indices R, T and S, respectively) are either the same or different from one another (models B or C with 12 or 14 parameters, respectively), and whether the stronger polarisabilities π, d reside on the arsenic ion or the gallium ion (models (i)

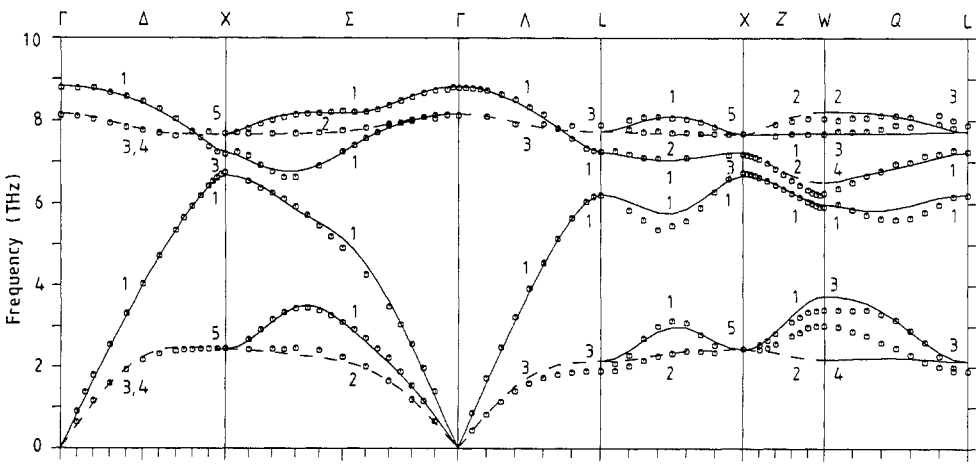

Figure 4. As figure 2, but the model calculations are with the deformation-dipole model DDM3.

or (ii), respectively). Dolling and Waugh argued that the models (i)—incorrectly stated as (ii)—were more physical in that the more negative arsenic ion (as it was found at the time) should be the more polarisable one. This criterion is met by our version C5(ii). In the other models the negative charge and the larger value of π and of d are distributed over the atoms in various ways, cf tables 8 and 9. The large number of parameters results in strong correlations among them, in particular among the parameters π_i and d_i (which describe the deformabilities) and—since they lead to indirect longer-range forces—between these and the direct second-neighbour force-constant parameters μ, ν and λ (but not δ, which is zero for a model with central potentials).

Figure 3 shows as an example the dispersion curves of the model with the lowest χ^2, C3(ii). The shell models B have too low LA and LO frequencies, and both the models B and C predict too low LA and too high TA frequencies at the L point. The splitting of the upper pair of branches along the X–W direction is too small in the B models. The two extra parameters of the C models lead to a better fit with values of χ^2 half of those of the B models. Apart from these differences the models (i) and (ii) give indeed nearly indistinguishable dispersion curves with only the order of some of the pairs of the dispersion curves along the X–W direction inverted.

4.1.3. Deformation-dipole model (DDM). The DDM accounts for the electronic polarisability α_i, but—compared to the shell model—only for part of the short-range deformability γ_i. This model is thus between the rigid-ion model and the shell model as is its χ^2.

The dispersion curves are shown in figure 4. The model does much better than the RIM but much worse than the shell models near the X and W points. A weak feature is the unsatisfactory description of the flat TA branches along all symmetry directions.

The value of the charge depends strongly on the choice of vectors $\boldsymbol{q}$ used in the fitting. The parameters β, Z and γ_2 are strongly correlated to each other and to many other parameters. It is most puzzling that the electronic polarisability α_1 comes out of the fitting routine to be negative as do most of the mechanical deformabilities γ_i, see table 7, and one must consider this solution as non-physical (note that differently from Kunc *et al* (1975b) we give the force constants in units of e^2/v and the polarisabilities α_i in units of v, as for the RIM, § 4.1.1).

Table 10. Overlap valence shell model parameters.

Parameter	OSM[a]	OSM5	OSM3
λ	48.1	38.7 ± 0.3	38.2 ± 0.3
k_θ	−2.74	−0.80 ± 0.07	−1.47 ± 0.07
k'_θ	0.80	0.90 ± 0.06	2.14 ± 0.05
$k_{r\theta}$	4.15	4.35 ± 0.10	4.28 ± 0.08
$k'_{r\theta}$	−4.75	−2.97 ± 0.13	−2.06 ± 0.14
Z_1	2.00	1.30 ± 0.03	1.16 ± 0.04
Y_1	7.12	13.75 ± 2.13	24.9 ± 5.3
Y_2	−2.51	−1.68 ± 0.10	−1.34 ± 0.12
k_1	515.2	3073 ± 993	7150 ± 3073
k_2	94.9	114.9 ± 1.9	121.9 ± 2.3
χ^2		47.9	28.2

[a] Kunc and Bilz (1967b).

4.1.4. Overlap valence shell model (OSM). The overlap valence shell model (Kunc and Bilz 1976a, b) includes bond-bending (with index θ) and bond-stretching valence forces (with index $r\theta$) and the effect of electronic polarisability. As in the case of the shell model, the polarisabilities are expressed in terms of (shell) charges Y_i and force constants k_i, which show a strong dependence on the manner in which the data are fitted. These parameters are strongly correlated to each other and to other parameters in a way which leaves the polarisabilities themselves rather unaffected. In fact, their values are of the order of the ones in the shell models (and the DDM), while the ionic charge is larger by an order of magnitude. Like in the original version the charge of the Ga shell comes out positive. See table 10.

The description of the dispersion curves, in particular along the Σ direction, is quite unsatisfactory, see figure 5. Improvement in this direction is parallelled by disimprovement near the X point. The crossing of the middle pair of dispersion curves along

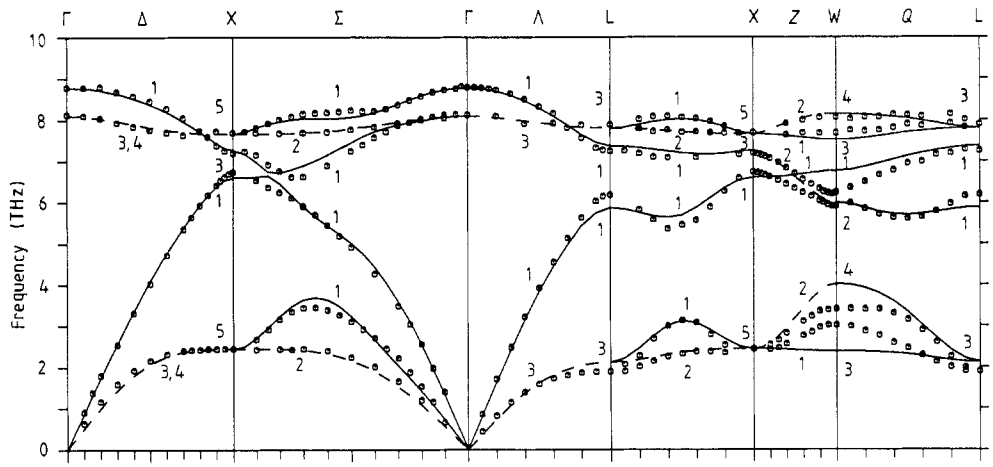

Figure 5. As figure 2, but the model calculations are with the overlap shell model OSM3.

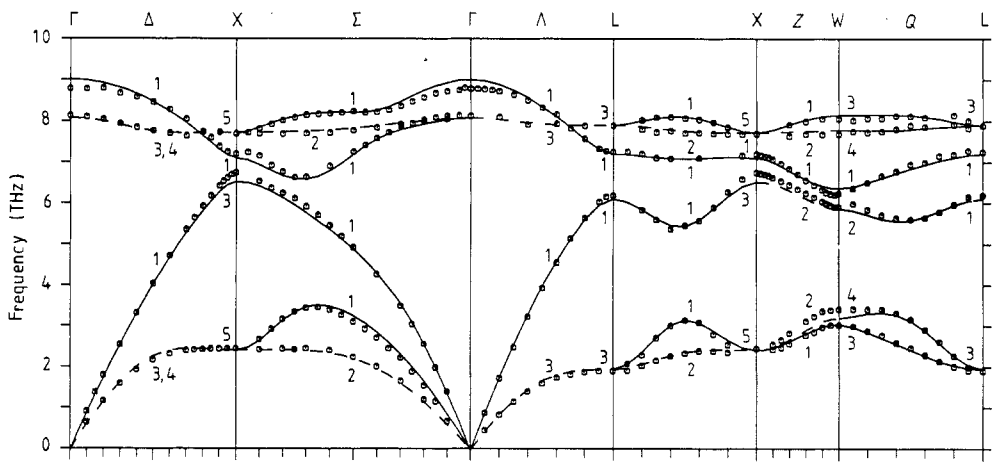

Figure 6. As figure 2, but the model calculations are with the bond-charge model BCM3.

the X–W direction does not occur for other parameter sets (which, for example, are obtained when the relative frequency deviations are minimised rather than the absolute ones).

4.1.5. Bond-charge model (BCM). In the bond-charge model the covalent bonding is simulated by bond charges between neighbouring ions, bound to the latter by short-range, Coulombic and angular forces. The latter are derived from a potential due to Keating (1966) with a strength parameter β. The ions themselves are assumed to be unpolarisable.

The bond-charge model is the only model which produces notable disagreement for the LO mode near the Γ point. This is probably due to the neglect of the electronic polarisability of the ions themselves (rather than the effect of the bond charges). This is not too surprising since the high-frequency dielectric constant ε_∞ is not reproduced by this model (Weber 1977). However, except for the LO branch near the Γ point the dispersion curves are most satisfactory, see figure 6. Most appealing is the fact that the model seems to be able to predict the dispersion in all other directions. This is expressed by the fact that the fit to five directions results in essentially the same model parameters as the fit to three, see table 11. On this ground the reliability of this model for the prediction of dispersion curves must be considered to be rather high. Finally, one should note that this model has the smallest number of parameters. Surprisingly, these relatively few parameters—with exception of the two parameters β_i of the Keating potentials—are highly correlated, which seems to be the reason for other minima found in parameter space with comparable values of χ^2.

Table 11. Bond charge model parameters.

Parameter	BCM[a]	BCM5	BCM3
$\varphi''_{\text{ion1-ion2}}$	18.48	15.43 ± 0.16	15.35 ± 0.15
$\varphi''_{\text{ion1-BC}}$	7.05	18.65 ± 0.44	18.68 ± 0.34
$\varphi''_{\text{ion2-BC}}$	48.15	103.32 ± 1.83	103.33 ± 1.40
β_1	5.36	2.40 ± 0.09	2.38 ± 0.07
β_2	8.24	8.89 ± 0.10	9.35 ± 0.10
Z^2/ε	0.187	0.415 ± 0.008	0.416 ± 0.005
χ^2	—	12.8	17.0

[a] Rustagi and Weber (1976) give combinations of these numbers.

Despite the deviations near the Γ and X points the value of χ^2 is already rather low when the model parameters are fitted to the dispersion curves along the three main symmetry directions. The bond-charge model is the only model for which χ^2 is lower for the fit to five directions than that for the fit to three (apparently due to the failure at just the Γ point).

4.2. Elastic constants

From the slopes of the acoustic-phonon dispersion curves at $\boldsymbol{q} = 0$ the elastic constants can be obtained. Neutron scattering is not a very useful technique for determining the

Table 12. Elastic constants c_{ij}, thermal fluctuations $\langle u_\alpha^2(\kappa)\rangle$ for $T = 295$ K and eigenvectors $\mathbf{e}(q)$.

Model	χ^2	c_{11}	c_{12}	c_{44}	$\langle u_\alpha^2(\text{Ga})\rangle$	$\langle u_\alpha^2(\text{As})\rangle$	$e(\text{X})$	$e(\text{L})$
		(10^{11} dyne cm^{-2})			(10^{-20} cm^2)			
RIM5	47.8	11.62	3.60	5.75	48.4	98.3	0	−0.70
RIM3	19.4	12.22	4.65	5.39	51.2	99.9	0	−0.76
DDM5	26.5	10.20	4.37	6.07	56.1	92.4	1	−0.97
DDM3	17.3	12.07	4.88	5.60	49.9	100.9	1	−0.96
B5(i)	23.5	13.49	7.00	5.39	66.9	85.6	1	0.86
B3(i)	20.5	13.35	6.97	5.25	66.3	84.1	1	0.86
B5(ii)	28.8	13.94	8.04	4.70	85.5	73.3	1	0.84
B3(ii)	25.7	13.33	7.38	4.71	83.0	71.1	1	0.83
C5(i)	14.7	12.11	7.48	5.05	69.4	88.4	1	0.90
C3(i)	12.0	12.37	6.72	5.56	65.3	86.5	1	0.92
C5(ii)	16.6	12.43	6.27	6.64	87.2	67.6	1	0.60
C3(ii)	11.4	12.48	6.28	5.72	86.6	66.4	1	0.58
OSM5	47.9	12.38	7.62	4.89	93.0	67.4	1	0.59
OSM3	28.2	13.17	7.78	4.61	91.6	67.1	1	0.66
BCM5	12.8	12.84	6.84	6.13	85.1	64.1	0	0.48
BCM3	17.0	12.99	6.86	6.23	85.1	63.9	0	0.48
Experiment		14.93[a]	7.10[a]	5.91[a]	79.0[c]	57.7[c]	1[f]	0.58(07)[f]
		12.11(04)[b]	5.48(17)[b]	6.04(02)[b]	78.3[d]	64.0[d]		
					92.0[e]	76.0[e]		

[a] Present work.
[b] Cottam and Saunders (1973).
[c] Shumski *et al* (1972).
[d] Gomm (1977).
[e] Pietsch (1981).
[f] Strauch and Dorner (1986).

elastic constants, and thus we have not paid particular attention to the low-frequency modes. Nevertheless, we have taken the experimental frequencies for $q \leqslant 0.3q_{\max}$ and have fitted ν^2 by a third-order polynomial in q^2 (a second-order polynomial gives nearly identical results). The results are given in table 12. Despite their large errors (about 10%) our results do not agree with the more accurate results from ultrasound techniques (Cottam and Saunders 1973). The 25 frequencies evaluated are probably either not enough or not exact enough or both.

Included in table 12 are the model elastic constants which are obtained from the slopes of the acoustic dispersion curves for $q \to 0$. (The slopes are simply obtained by fitting a parabola to the values of ν^2 as a function of q^2 for q_α equal to 0.04, 0.06 and 0.1.) The results of the model calculations show a fair amount of scatter around the ultrasonic values; they tend to be smaller than the values obtained from the experimental dispersion curves. In particular the values of c_{44} are definitely too low in the OSM and B(ii) model, and c_{12} is too small in the RIM and DDM. Since it is somewhat difficult to estimate the errors in the theoretical frequencies, we have not given errors on the theoretical elastic constants. Actually, one should calculate the elastic constants directly from the model parameters.

4.3. Debye–Waller factor

The Debye–Waller exponent (2) can be expressed in terms of thermal fluctuations of

the atomic displacements

$$\langle u_\alpha^2(l\kappa)\rangle = \tfrac{1}{3}\langle \boldsymbol{u}^2(l\kappa)\rangle \tag{4}$$

for which model results are included in table 12. Only half of the models have the expected slightly larger value for the (lighter) gallium atom, even though the relative difference is much larger than the relative mass difference. For a comparison with experimental data we have used a temperature of 295 K in the Bose factor, cf equation (2), even though the eigen-solutions refer to $T \simeq 0$. With an approximate 1% decrease in the frequencies for room temperature, the actual mean-square displacements (for room temperature) are expected to be larger by about 2%. The experimental data quoted in table 12 are from the analysis of x-ray data, and comparison must thus be made with caution.

4.4. Phonon eigenvectors at the X and L points

Also included in table 12 are the calculated eigenvectors of the longitudinal phonons at the X point and the L point. These eigenvectors have been determined experimentally (Strauch and Dorner 1986) from neutron scattering intensities. The eigenvectors of these phonons can be written in the form

$$\begin{aligned} \boldsymbol{e}(\mathrm{Ga}|\boldsymbol{q}, \mathrm{LO}) &= e(\boldsymbol{q})\hat{\boldsymbol{e}} & \boldsymbol{e}(\mathrm{As}|\boldsymbol{q}, \mathrm{LO}) &= -[1 - e^2(\boldsymbol{q})]^{1/2}\hat{\boldsymbol{e}} \\ \boldsymbol{e}(\mathrm{Ga}|\boldsymbol{q}, \mathrm{LA}) &= [1 - e^2(\boldsymbol{q})]^{1/2}\hat{\boldsymbol{e}} & \boldsymbol{e}(\mathrm{As}|\boldsymbol{q}, \mathrm{LA}) &= e(\boldsymbol{q})\hat{\boldsymbol{e}} \end{aligned} \tag{5}$$

where $\hat{\boldsymbol{e}}$ is the unit vector along $\boldsymbol{q}$.

Symmetry requires that e has the value of either 0 or 1 at the X point. The experimental value of $e = 1$ means that the lighter gallium atom vibrates in the higher-frequency (LO) mode (X_3 representation); the arsenic atom is at rest; then the other (LA) mode belongs to the X_1 representation. Most of the model predictions are in agreement with experiment. Another compilation of X-point eigenvectors has been presented by Kunc and Martin (1983); they find $e = 0$ for the models B(i) and C(ii) with the parameters of Dolling and Waugh (1965).

As far as the eigenvector $\boldsymbol{e}$ for the L point is concerned, the experiment gave clearly $e > 0$, which is not reproduced by the RIM and DDM. The conclusion about the magnitude, $e = 0.58 \pm 0.07$, was not as clear cut; a value of 0.81 did not seem totally improbable. Except for the RIM and DDM, the theoretical results scatter, in fact, around either of these two numbers. The OSM and C(ii) models give agreement with the former, more probable, value of e, the B(i), B(ii) and C(i) models with the latter.

Tamura (1984, 1986) in his model studies of the lattice dynamics of GaAs finds an eigenvector $|e| = 0.22$ at the L point, much smaller in magnitude than ours, for the DDM and an eigenvector similar to ours for the RIM (Tamura 1986) and for the OSM (Tamura 1984).

The eigenvector of our BCM is in disagreement with experiment at the X point; the version of the BCM used by Lax *et al* (1981) has the correct value at the X point. It is possible that inclusion of electronic polarisability effects (Labrot *et al* 1988) changes the dynamics of these phonons together with that of the optical phonons at the Γ point.

There are also quantum-mechanical results for the eigenvectors: Kunc and Martin (1983) find $e(\mathrm{X}) = 1$, and Kunc and Hagège (1985) obtain $e(\mathrm{L}) = 0.76$; Falter *et al* (1985) find $e(\mathrm{X}) = 1$ and $e(\mathrm{L}) = 0.83$.

4.5. W-point phonons

Similarly to the results for the X-point phonons of the preceding section, the gallium atom is at rest in the W_1 mode while the other vibrates, and vice versa for the W_2 mode. It is not *a priori* clear which of these two modes at X and W has the higher frequency. However, all our model calculations have the result that the X_1 and W_1 modes belong to the same (Z_1) branch. Note that for wavevectors between X_1 and W_1 the gallium atom is not at rest, even though the amplitude is small. A corresponding result is found for the X_3 and W_2 modes with the arsenic atom at rest except for the RIM and DDM. For the latter, the W_2 mode is on the uppermost Z_2 branch; this seems to be related to the wrong eigenvectors at L.

We have tried to assign the symmetry to the experimental W-point phonons by comparing the scattering intensities to results of model calculations. Let the six modes at W be numbered from 1 to 6 from bottom to top; rather than investigating the scattering function $S(\boldsymbol{Q}, \omega)$ we have calculated the reduced intensity

$$I_{qj}(\boldsymbol{Q}) = \frac{\omega}{(1 + n_\omega)Q^2} \int \mathrm{d}\Omega \, S(\boldsymbol{Q}, \Omega) \tag{6}$$

(integrated over just the one-phonon peak at $\omega = \omega(\boldsymbol{qj})$) since it does not contain explicit frequency factors (in fact, n_ω is practically equal to zero); also, except for the Debye–Waller factor (2), $I_{qj}(\boldsymbol{Q})$ should fulfil a sum rule (see, e.g., Strauch and Dorner 1986, Dorner and Strauch 1990). Even though it will turn out largely unsuccessful anyway, this analysis must remain tentative since the experimental data for the W point are taken at only very few momentum transfers, and the intensities can thus not be checked for consistency (i.e., against spurious contamination).

The experimental intensity ratio I_2/I_1 for the lowest-frequency pair is found to be 0.8 at $\boldsymbol{Q} = (2.5, 1, 0)$. All model intensities give a ratio <1.0, the RIM and the DDM giving values too small by factors 4 and 2, respectively. The shell-model results are closest to the experimental value, but the shell models (i) predict the W_4 mode with the lowest frequency and the models (ii) the W_3 mode. An assignment of those two modes is thus not possible so far.

Likewise, no conclusion is possible about the uppermost pair of modes. The experimental intensity ratio I_6/I_5 is equal to 0.8 for $\boldsymbol{Q} = (0, 5.5, 1)$ and <1.8 for $\boldsymbol{Q} = (5, 0.5, 0)$. The shell models (i) are closest to the latter value, and the shell models (ii) are closest to the former; the results of the RIM, DDM and OSM are off by factors of 2 to 50.

As far as the middle pair of modes is concerned, the experimental intensity ratio I_4/I_3 of about 1.5 is matched by the DDM and the shell models with theoretical values of about 1.3, and in all these models the mode number 3 has W_1 symmetry. The DDM is unreliable because of the results for the other intensities (I_6/I_5, I_2/I_1), but the assignment from the unanimous results of the shell models is probably correct. In these models the mode number 4 is of W_2 symmetry. These two assignments of the W phonons (and thus the Z branches) seem to be the only safe ones (out of a total of six).

4.6. Summary of the model results

We are not sure whether or not lower minima of χ^2 exist. In fact, the four-shell models of Dolling and Waugh (1965) are actually only two, each with two minima. Dolling and

Waugh did not find any other minimum for their model B in an extensive search, and we simply used the originally published numbers as an initial guess. We did find other local minima for most of the models. For the BCM a local minimum was found with a parameter set close to that of Rustagi and Weber (1976); this set is quite different from the one for BCM3 or BCM5 given in table 11 but the eigen-solutions are very similar, a major difference occurring in e(L) which is equal to 0.41.

Irrespective of whether the theoretical dispersion curves are fitted to three or five symmetry directions it turned out that the model parameters (and thus the dispersion curves) are more or less the same for a given model (a notable exception are the DDM and, less markedly, the shell models). Naively, one would be tempted to conclude that a model fitted to the data of just the three directions Δ, Σ and Λ can be considered as reliable to predict the phonon dispersion curves in all other directions. This is true at least for the two directions L–X and L–W: inclusion of these latter two directions only doubles the value of χ^2 for the RIM, DDM and OSM, for the other models χ^2 is essentially unchanged. The results for the direction X–W, however, contradict this assumption.

First, none of the models seems to be able to reproduce all six W-point phonon frequencies to a quantitatively and sometimes even qualitatively satisfying degree except DDM5 (which has other drawbacks, see § 4.1.3) and possibly C(i).

Secondly, there seems to be a qualitative uncertainty: the dispersion curves along the X–W direction (with two possible representations) come in three close-lying pairs (partially degenerate at X) (see the figures) every pair containing one mode of both representations. There are, in principle, eight ways of an arrangement of the three dispersion-curve pairs along X–W. Six of them are achieved by the eight models, the models DDM, B(i) and C(i) giving the same sequence, see § 4.5 above. A symmetry assignment of the W-point phonons would be rather illuminating but, as stated above, is quite involved experimentally.

Finally, none of the models can properly describe the pure TA branch along Σ except possibly the BCM, which, however, is the only one which is badly off for the LO mode near the Γ point.

No clear picture seems to evolve other than for the order of magnitude of the ionic charge, the strength of interionic forces or the value of the polarisability. This is true even of the four-shell models.

The rigid-ion model gives a fair description of the phonon dispersion curves, but seems to be unphysical, as is demonstrated by unphysical eigenvectors.

The deformation-dipole model is susceptible to unphysical parameter sets.

The shell model is quite physical in that it includes the effect of polarisation; but the sophisticated version with its huge number of parameters must be considered mostly as a means of interpolation (of the phonon frequencies) rather than a physical description. This is expressed in a large scatter of the model parameters for the different versions, and this leads, among others, to various combinations of eigenvectors. See table 12.

It seems essential for homopolar substances to include bond-bending forces (rather than to simulate them by second-neighbour or other forces). This is done in the overlap valence shell model and in the bond-charge model. The former, however, gives a comparatively poor description of the dispersion curves and of c_{44}. The latter seemingly neglects some ionic polarisability. The bond-charge model is the one with the fewest (even though highly correlated) model parameters, and it is the one in closest agreement with the dispersion curves. We expect that a combination of the bond-charge and a simple shell model will give a superior description of the phonon dynamics. Such studies are under way (Labrot *et al* 1988).

5. Conclusions

We have obtained phonon dispersion curves of GaAs for phonon propagation in six different directions, twice as many as had been known to date; in addition, the data now carry much smaller errors.

None of eight models investigated is able to reproduce the whole of the dispersion curves to a satisfactory degree. This is true even of the main symmetry directions. Major discrepancies, however, have become apparent in the newly-investigated, off-symmetry directions. In particular in the W–(Z)–X and W–(Q)–L directions there is even qualitative disagreement among the models, and since the model scattering intensities are at variance the symmetry of the W (and Z) phonons remains unassigned at present. (There is only one representation for the Q direction.) In the bond-charge model, however, the larger deviations occur for the main symmetry directions, and it will be interesting to see whether a modification of this model can remove these discrepancies without spoiling the agreement in the off-symmetry directions.

Acknowledgments

We are very much indebted to Dr K Kunc and Dr A Mazur for sending us computer codes for the various lattice-dynamical models and to Dr Stath of the Siemens Laboratory for donating the crystal.

References

Bross H 1989 private communication
Cochran W 1959 *Phil. Mag.* **4** 1082
Cottam R I and Saunders G A 1973 *J. Phys. C: Solid State Phys.* **6** 2105
Dolling G and Waugh J L T 1965 *Lattice Dynamics* ed. R F Wallis (Oxford: Pergamon) p 19
Dorner B 1972 *Acta Crystallogr.* A **28** 319
Dorner B and Strauch D 1990 *J. Phys.: Condens. Matter* **2** 1475–83
Falter C, Ludwig W and Selmke M 1985 *Phonon Physics* ed. J Kollár, N Kroó, N Menyhárd and T Siklós (Singapore: World Scientific) p 962
Fasol G, Tanaka M, Sakaki H and Horikoshi Y 1988 *Phys. Rev.* B **38** 6056
Gomm M 1977 Dissertation Erlangen-Nürnberg, unpublished
Herman F 1959 *J. Phys. Chem. Solids* **8** 405
Ishibashi A, Itabashi M, Mori Y, Kaneko K, Kawado S and Watanabe N 1986 *Phys. Rev.* B **33** 2887
Jusserand B and Cardona M 1989 *Light Scattering of Solids V (Springer Topics in Solid State Physics 66)* ed. M Cardona and G Güntherodt (Berlin: Springer) p 49
Jusserand B and Paquet D 1986 *Phys. Rev. Lett.* **56** 1752
Keating P N 1966 *Phys. Rev.* **145** 637
Kunc K, Balkanski M and Nusimovici M A 1975a *Phys. Rev.* B **12** 4346
—— 1975b *Phys. Status Solidi* b **72** 229
Kunc K and Bilz H 1976a *Proc. Int. Conf. Neutron Scattering* ed. R M Moon (Gatlinburg, Tennessee: ORNL) p 195
—— 1976b *Solid State Commun.* **19** 1027
Kunc K and Hagège P 1985 *Phonon Physics* ed. J Kollár, N Kroó, N Menyhárd and T Siklós (Singapore: World Scientific) p 943
Kunc K and Martin R M 1983 *Ab initio Calculations of Phonon Spectra* ed. J T Devreese, V E van Doren and P E van Kamp (New York: Plenum) p 65
Kunc K and Nielsen O H 1979a *Comput. Phys. Commun.* **16** 181
—— 1979b *Comput. Phys. Commun.* **17** 413
Labrot M T, Mayer A P and Wehner R K 1988 *Verhandl. DPG (VI)* **23** Dy-14.47

Lax M, Narayanamurti V, Hu P and Weber W 1981 *J. Physique Coll.* **42** C6 161
Molinari E, Fasolino A and Kunc K 1986 *Phys. Rev. Lett.* **56** 1751
Pietsch U 1981 *Phys. Status Solidi* b **103** 93
Press W H, Flannery B P, Teukolsky S A and Vetterling W T 1986 *Numerical Recipes* (Cambridge: Cambridge University Press)
Rustagi K C and Weber W 1976 *Solid State Commun.* **18** 673
Shumskii M G, Bublik V T, Gorelik S S and Gurevich M A 1971 *Kristallografiya* **16** 779 (1972 *Soviet Phys.—Crystallogr.* **16** 674)
Sinha S K 1973 *CRC Crit. Rev. Solid State Sci.* **3** 273
Sood A K, Menéndes J, Cardona M and Ploog K 1985 *Phys. Rev. Lett.* **54** 2111
—— 1986 *Phys. Rev. Lett.* **56** 1753
Strauch D and Dorner B 1986 *J. Phys. C: Solid State Phys.* **19** 2853
Tamura S 1984 *Phys. Rev.* B **30** 849
—— 1986 *Phonon Scattering in Condensed Matter* vol 5 ed. A C Anderson and J P Wolfe (Berlin: Springer) p 288
Waugh J L T and Dolling G 1963 *Phys. Rev.* **132** 2410
Weber W 1974 *Phys. Rev. Lett.* **33** 371
—— 1977 *Phys. Rev.* B **15** 4789
Woods A D B, Cochran W and Brockhoues B N 1960 *Phys. Rev.* **119** 980
Woods A D B, Brockhoues B N, Cowley R A and Cochran W 1963 *Phys. Rev.* **131** 1025